# Optimization of Asymmetrical Difference Pattern With Memetic Algorithm

Song-Han Yang and Jean-Fu Kiang

***Abstract*—A memetic particle swarm optimization (MPSO) algorithm is applied to fine-tune the asymmetrical difference pattern of a linear array, which is useful for tracking targets, for example, in radar applications. The side-lobe level of the asymmetrical difference pattern with various peak differences can be successfully reduced, while maintaining the desired squint angle and the side-lobe difference. Conventional PSO, genetic algorithm (GA) and memetic GA (MGA) have also been applied, with the initial conditions of uniformly-excited and Bayliss linear arrays, to compare their performance of optimization.**

***Index Terms*—Evolutionary computation, phased arrays, radar tracking.**

## I. Introduction

The difference patterns generated by phased arrays are useful for tracking and searching in radar applications [1]. For example, maritime radars have been used to detect ships, land targets, and nearby obstacles. In practice, asymmetric difference patterns are widely used to separate the echoes from opposite sides of the pointing direction.

The difference patterns considered in many works are symmetrical [2]–[5]. M. Satyanarayana *et al.* apply an interpolation technique to determine the amplitude and phase of the array elements in order to generate an asymmetrical difference pattern [2]. However, this technique can not simultaneously take care of other constraints on the characteristics of the difference pattern, such as directivity, squint angle between peaks and side-lobe level. On the other hand, analytical methods are often stuck in a local optimum, especially when the problem is complex [2].

Evolutionary algorithms (EA's) have been successfully applied to find the global optimum solution in complex electromagnetic problems [6], [7]. R. L. Haupt applies a genetic algorithm (GA) to synthesize thinned arrays [8]. V. Murino *et al.* adopt a simulated annealing (SA) algorithm to reduce the side-lobe level by adjusting the position and weighting coefficient of the elements [9]. D. G. Kurup *et al.* synthesize the desired pattern by using a differential evolution strategy (DES) to adjust the position and/or phase of the elements [10]. M. M. Khodier *et al.* apply a particle swarm optimization (PSO) algorithm to optimize the spacings between elements in order to minimize the side-lobe level and to control the null locations [11]. O. Quevedo-Teruel *et al.* control the side-lobe level of a thinned array using an ant colony optimization (ACO) method [12]. G. Oliveri *et al.* combine the EA's and *a priori* information of the almost difference sets (ADS's) to improve the performance of an array [13], [14].

In this work, a memetic algorithm (MA) [15] is adopted to optimize the difference pattern of a linear array. The memetic algorithm is viewed as a hybrid of a global searching algorithm and a local searching one. Unlike the conventional memetic algorithm based on GA (MGA) [16], the PSO algorithm is combined with a local search to derive a memetic particle swarm optimization (MPSO) algorithm [17].

Manuscript received April 06, 2013; revised September 22, 2013; accepted January 17, 2014. Date of publication January 24, 2014; date of current version April 03, 2014. This work was sponsored by the National Science Council, Taiwan, ROC, under contract NSC 100-2221-E-002-232.

The authors are with the Department of Electrical Engineering and the Graduate Institute of Communication Engineering, National Taiwan University, Taipei, Taiwan (e-mail: jfkiang@ntu.edu.tw).

Digital Object Identifier 10.1109/TAP.2014.2302440

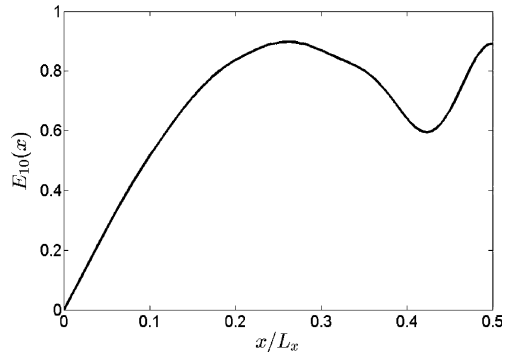


Fig. 1. Bayliss line-source distribution, $N_b = 10$ and $\mathrm{SLL} = 20$ dB.

The MPSO is adopted in this work to generate the required asymmetrical difference patterns, with a linear Bayliss array and a uniformly-excited array, respectively, as the initial guess. The implementation of a linear Bayliss array with uniformly spaced elements is briefly described in Section II, the MPSO algorithm is briefly reviewed in Section III. The optimization performance with the initial guess of a uniformly excited linear array and a Bayliss linear array is presented in Section IV, using PSO, MPSO, GA and MGA. The conclusion is drawn in the last section.

## II. Review of Linear Bayliss Array

Consider a continuous line source of length $L_x$, aligned along the $x$ axis. Its far-field pattern is required to have a null in the boresight direction, plus $N_b - 1$ nulls within the angular range of $0 < \theta \leq 90°$; and all the side-lobes are below a specific level, SLL. The Bayliss line-source distribution is designed to fulfill these requirements, with the distribution of [18]

$$E_{N_b}(x) = \sum_{m=0}^{N_b-1} B_m \sin\left[(2m+1)\pi \frac{x}{L_x}\right], \quad \left|\frac{x}{L_x}\right| \leq \frac{1}{2} \tag{1}$$

which is anti-symmetric with respect to the center, the coefficients take the form

$$B_m = \frac{(-1)^m (m+0.5)^2}{2} \frac{\prod_{n=1}^{N_b-1} [1-(m+0.5)^2/Z_n^2]}{\prod_{n=0, n\neq m}^{N-1} [1-(m+0.5)^2/(n+0.5)^2]}$$

with

$$Z_n = \begin{cases} (N_b+0.5)\sqrt{\dfrac{\xi_n^2}{A^2+N_b^2}}, & 1 \leq n \leq 4 \\ (N_b+0.5)\sqrt{\dfrac{A^2+n^2}{A^2+N_b^2}}, & 5 \leq n \leq N_b-1 \end{cases}$$

and

$$\xi_n = \sum_{p=0}^{4} C_p^n (\mathrm{SLL})^p$$

$$A = \sum_{p=0}^{4} C_p^A (\mathrm{SLL})^p$$

where SLL is in unit of dB, and the coefficients, $C_p^\alpha$'s, can be found in [19]. Fig. 1 shows an example of the Bayliss line-source distribution, with $N_b = 10$ and $\mathrm{SLL} = 20$ dB.

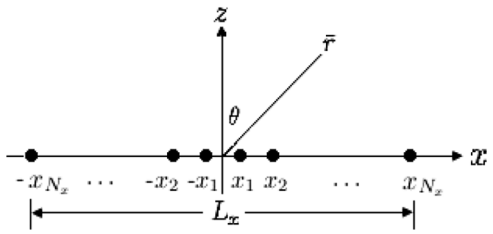


Fig. 2. Geometry of a linear array of length $L_x$, with $2N_x$ elements at uniform spacing of $d_x$.

Fig. 2 shows a linear array of length $L_x$, aligned along the $x$ axis, which is composed of $2N_x$ elements at a uniform spacing of $d_x$. The array factor in describing its far-field pattern can be expressed as

$$\begin{aligned}\mathrm{AF}(\theta) &= \sum_{n=-N_x}^{-1} a_n e^{j(n+1/2)kd_x\cos\theta} + \sum_{n=1}^{N_x} a_n e^{j(n-1/2)kd_x\cos\theta} \\ &= \sum_{n=1}^{N_x} a_n \sin[kx_n\cos\theta] \end{aligned} \quad (2)$$

where $a_n$ is the amplitude of the $n$th radiating element, located at $x_n = (n-1/2)d_x$; and $a_n = -a_{-n}$. A Bayliss linear array is formed if the amplitudes, $a_n$'s, are sampled from the Bayliss line-source distribution [20]. The far-field pattern of a linear Bayliss array approaches that of an ideal Bayliss line-source distribution when the density of elements increases.

## III. Review of Memetic Algorithm

As the genes carry the instructions to construct proteins, the memes carry the instructions to behave in a specific way [15]. Charles Darwin coined the term, meme, as the fundamental unit of cultural transmission or imitation that may be passed on from generation to generation. Inspired by the ideas of genes and memes, the memetic algorithm (MA) is made of a population-based global search (genes) and a local improvement procedure (memes). The MA is expected to take advantage of the fast convergence of EA's, while avoiding the flaw of being trapped in local optima.

The evolutionary programming (EP), one variation of EA's, bears the advantages of simplicity, ease of implementation and flexibility [21]. The particle swarm optimization (PSO) algorithms are inspired by mimicking a food-searching swarm [7], and belong to the school of evolutionary programming. The memetic PSO (MPSO) is one of the PSO algorithms, equipped with a local search technique [17].

In a typical PSO algorithm, the velocity is updated as [7]

$$\begin{aligned}\bar{\bar{V}}^{(\ell+1)} = w^{(\ell)}\bar{\bar{V}}^{(\ell)} &+ C_1\bar{\bar{U}}_1^{(\ell)} \otimes \left(\bar{\bar{P}}^{(\ell)} - \bar{\bar{X}}^{(\ell)}\right) \\ &+ C_2\bar{\bar{U}}_2^{(\ell)} \otimes \left(\bar{\bar{G}}^{(\ell)} - \bar{\bar{X}}^{(\ell)}\right) \end{aligned} \quad (3)$$

where $\otimes$ means component-wise product, $C_1$ and $C_2$ are empirical constants; and the $\bar{\bar{U}}^{(\ell)}$ matrix in the $\ell$th iteration is composed of random numbers picked from the interval [0, 1]; $w^{(\ell)}$ is the inertia weight in the $\ell$th iteration; $X_{\min}$ and $X_{\max}$ are the lower and the upper limits, respectively, of the initial range; and

$$V_{\max} = \alpha(X_{\max} - X_{\min})$$

with $\alpha$ a random number picked from the interval [0, 1].

With $M$ particles, each of dimension $N$, the position and velocity matrices can be defined as

$$\bar{\bar{X}} = \begin{bmatrix} x_{11} & x_{12} & \cdots & x_{1N} \\ x_{21} & x_{22} & \cdots & x_{2N} \\ \vdots & \vdots & \cdots & \vdots \\ x_{M1} & x_{M2} & \cdots & x_{MN} \end{bmatrix}$$

$$\bar{\bar{V}} = \begin{bmatrix} v_{11} & v_{12} & \cdots & v_{1N} \\ v_{21} & v_{22} & \cdots & v_{2N} \\ \vdots & \vdots & \cdots & \vdots \\ v_{M1} & v_{M2} & \cdots & v_{MN} \end{bmatrix}$$

Similarly, the matrix of personal best positions is defined as

$$\bar{\bar{P}} = \begin{bmatrix} p_{11} & p_{12} & \cdots & p_{1N} \\ p_{21} & p_{22} & \cdots & p_{2N} \\ \vdots & \vdots & \cdots & \vdots \\ p_{M1} & p_{M2} & \cdots & p_{MN} \end{bmatrix}$$

Each of the $M$ particles searches for its optimum position in the $N$-dimensional space, based on a fitness function. During the $\ell$th iteration, a particle updates its personal best position (pbest), recorded in matrix $\bar{\bar{P}}$, if the fitness function at the new position is better than that at the old one. Next, if its associated vector in matrix $\bar{\bar{P}}$ renders a better fitness function than the group best position (gbest), $\bar{g}$, the latter will be replaced by the former.

For the convenience of coding, the matrix $\bar{\bar{G}}$ is constructed by placing the $\bar{g}$ vector in each of its $M$ rows. The choices of boundary condition, search range and dynamic range are critical to the performance of a PSO algorithm [22]. In this work, an invisible boundary condition (IBC) is chosen.

A local search is executed over the whole population in the memetic algorithm [16]. In [17], a gradient-free local search is applied only to the personal best positions in matrix $\bar{\bar{P}}$ and the group best position in matrix $\bar{\bar{G}}$, excluding the positions in matrix $\bar{\bar{X}}$. More details about PSO, MPSO, GA and MGA algorithms can be found in [7], [15]–[17].

## IV. Optimization of Difference Patterns

We are also curious about the difference between the PSO-type algorithms and the GO-type counterparts, at least in the array optimization problems. The PSO-type is inspired by moving particles, with more or less continuous tracks. On the other hand, the cross-over and mutation processes in the GO-type tend to create more abrupt change in members of the population. Hence, the performance of PSO, MPSO, GA and MGA will be presented and compared in this section.

As we know of, the initial condition may affect the outcome of an optimization algorithm. We also wonder how the PSO-type and the GO-type algorithms respond to the initial condition. Hence, two types of amplitude distribution are considered as the initial condition before optimization: A uniformly excited linear array and a Bayliss linear array. The former one provides no *a priori* information, but the latter one has the basic characteristics close to the desired pattern.

### A. Bayliss Array as Initial Condition

Consider a uniformly spaced linear array, consisted of 20 elements ($L_x = 10\lambda$ and $N_x = 10$). The initial amplitude of these elements is sampled from a continuous Bayliss array with $N_b = 10$.

Two fitness functions are considered. The first one is defined as

$$\begin{aligned} f(\bar{w},\bar{\psi}) = P(\Omega|\bar{w},\bar{\psi}) &+ K_1|\mathrm{PD}(\bar{w},\bar{\psi}) - \mathrm{PD}_d| \\ &+ K_2|\mathrm{SA}(\bar{w},\bar{\psi}) - \mathrm{SA}_d| \end{aligned} \quad (4)$$

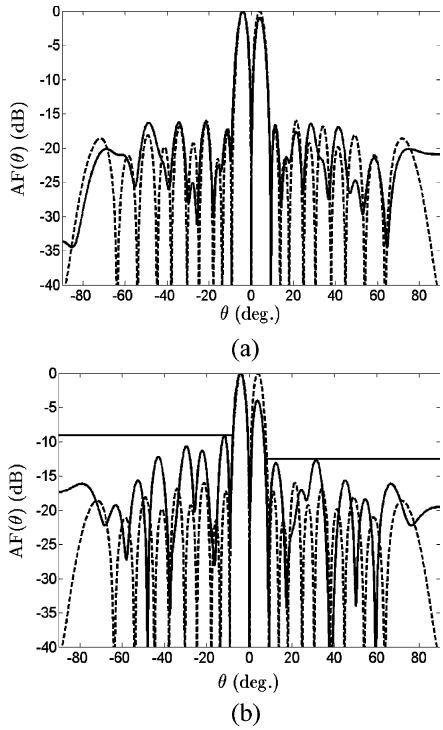


Fig. 3. Difference field pattern with $L_x = 10\lambda$ and $N_x = 10$; —: optimized from Bayliss array, – – –: initial Bayliss array with $N_b = 10$; (a) $\mathrm{PD}_d = 1$ dB (b) $\mathrm{PD}_d = 4$ dB and $\mathrm{SD}_d = 3.5$ dB.

TABLE I
PARAMETERS USED IN THE PSO AND MPSO ALGORITHM

| $M$ | $N$ | $\alpha$[7] | $C_1$[7] | $C_2$[7] | $K$ | $K_1$ | $K_2$ | $K_3$ |
|---|---|---|---|---|---|---|---|---|
| 30 | 40 | 0.2 | 2 | 2 | $10^6$ | $10^6$ | $10^6$ | $10^6$ |

where $K_1$ and $K_2$ are empirical weighting factors; $\bar{w} = [w_1, w_2, \cdots, w_{2N_x}]^t$ contains the amplitude of all the elements; and $\bar{\psi} = [\psi_1, \psi_2, \cdots, \psi_{2N_x}]^t$ contains the phase of all the elements.

In (4), the first term on the right hand side is designed to minimize the side-lobe level, where $\Omega$ indicates the angular location of the maximum side-lobe. The second term on the right hand side is designed to achieve the desired peak difference, $\mathrm{PD}_d$ (in dB), assuming the left peak is higher than the right one, without loss of generality. The third term on the right hand side is designed to achieve the desired squint angle, $\mathrm{SA}_d$ (in degrees). The best results out of 10 trials are adopted as the optimal solution. Table I lists the parameters used in the MPSO algorithm. The phase is searched within $(-\pi, \pi]$, and the amplitude is searched within $(0, 1]$.

The simulation results are shown in Fig. 3 and summarized in Table II. The results shown in Fig. 3(a), using the MPSO, is better than those in Fig. 5 of [2], in terms of squint angle (SA), beamwidth (BW), side-lobe level (SLL) and side-lobe difference (SD). The optimized results with several different peak differences and similar squint angle are also listed. It is observed that when a higher peak difference is imposed, the side-lobe level usually becomes higher.

A second fitness function is defined as

$$\begin{aligned} f(\bar{w}, \bar{\psi}) = {} & P_L(\Omega_L|\bar{w}, \bar{\psi}) + K_1|\mathrm{PD}(\bar{w}, \bar{\psi}) - \mathrm{PD}_d| \\ & + K_2|\mathrm{SA}(\bar{w}, \bar{\psi}) - \mathrm{SA}_d| \\ & + K_3 \max\{0, \mathrm{SD}_d - [P_L(\Omega_L|\bar{w}, \bar{\psi}) \\ & - P_R(\Omega_R|\bar{w}, \bar{\psi})]\} \end{aligned} \quad (5)$$

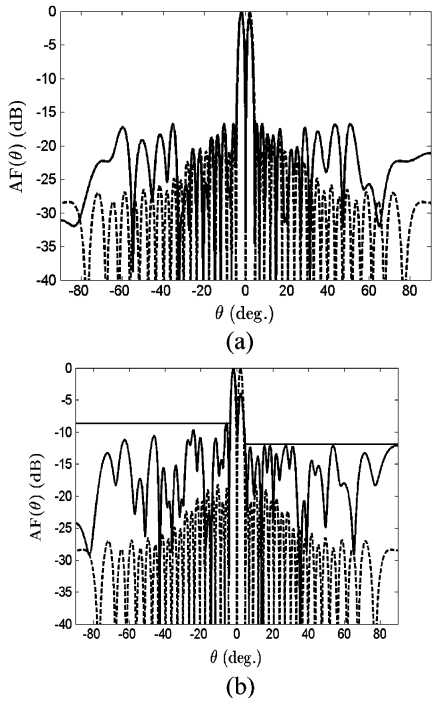


Fig. 4. Difference field pattern with $L_x = 20\lambda$ and $N_x = 20$; —: optimized from Bayliss array, – – –: initial Bayliss array with $N_b = 10$; (a) $\mathrm{PD}_d = 1$ dB, (b) $\mathrm{PD}_d = 4$ dB and $\mathrm{SD}_d = 3.5$ dB.

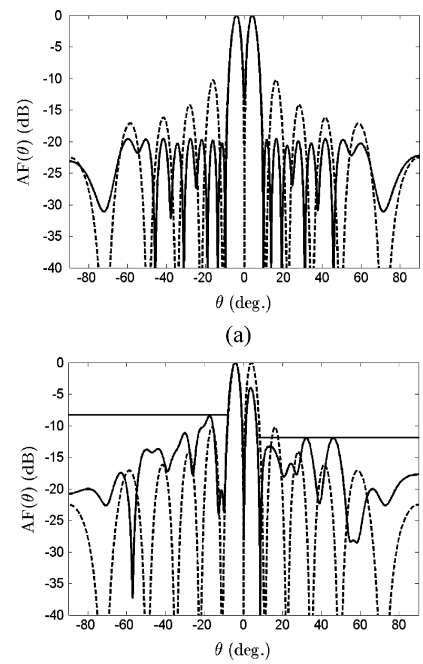


Fig. 5. Difference field pattern with $L_x = 10\lambda$ and $N_x = 10$; —: optimized array, – – –: initial uniformly excited array; (a) $\mathrm{PD}_d = 1$ dB, (b) $\mathrm{PD}_d = 4$ dB and $\mathrm{SD}_d = 3.5$ dB.

where $K_3$ is another empirical weighting factor; $\Omega_L$ and $\Omega_R$ are the angular locations of the maximum side-lobe on the left and the right hand side, respectively; $P_L$ and $P_R$ are power level at $\Omega_L$ and $\Omega_R$, respectively. In (5), the fourth term on the right hand side is designed to constrain the maximum side-lobe difference between $P_L$ and $P_R$ to $\mathrm{SD}_d$.

TABLE II
COMPARISON OF RESULTS IN Fig. 5 IN [2] AND Fig. 3

| Source | $PD_d$ (dB) | $SA_d$ (deg.) | PD (dB) | SA (deg.) | BW (deg.) | SLL (dB) | SD (dB) |
|---|---|---|---|---|---|---|---|
| $N_x = 10$ | | | | | | | |
| Fig. 5 [2] | none | none | 1.00 | 9.59 | 23.06 | −11.53 | 1.00 |
| Initial Bayliss pattern | none | none | 0.00 | 8.00 | 18.60 | −16.01 | 0.00 |
| Optimized pattern 1 | 0.00 | 8.00 | 0.00 | 8.00 | 19.40 | −19.82 | 0.00 |
| Optimized pattern 2 (Fig. 3 (a)) | 1.00 | 8.00 | 1.00 | 8.00 | 19.10 | −16.25 | 0.18 |
| Optimized pattern 3 | 2.00 | 8.00 | 2.00 | 8.00 | 20.80 | −13.74 | 0.28 |
| Optimized pattern 4 | 4.00 | 8.00 | 4.00 | 8.00 | 20.90 | −9.42 | 1.32 |
| Optimized pattern 5 (Fig. 3 (b)) | 4.00 | 8.00 | 4.00 | 8.00 | 18.00 | −9.12 | 3.54 |
| $N_x = 20$ | | | | | | | |
| Initial Bayliss pattern | none | none | 0 | 4.00 | 9.40 | −18.22 | 0.00 |
| Optimized pattern 1 | 0.00 | 4.00 | 0.00 | 4.00 | 9.50 | −19.84 | 0.00 |
| Optimized pattern 2 (Fig. 4 (a)) | 1.00 | 4.00 | 1.00 | 4.00 | 9.30 | −16.74 | 0.00 |
| Optimized pattern 3 | 2.00 | 4.00 | 2.00 | 4.00 | 10.20 | −13.95 | 0.00 |
| Optimized pattern 4 | 4.00 | 4.00 | 4.00 | 4.00 | 9.40 | −13.31 | 0.00 |
| Optimized pattern 5 (Fig. 4 (b)) | 4.00 | 4.00 | 4.00 | 4.00 | 10.10 | −8.60 | 3.50 |

TABLE III
AMPLITUDES AND PHASES OF EXCITATION TO GENERATE THE FIELD PATTERN IN Fig. 3(a) AND (b)

| | | | | | | | | | | |
|---|---|---|---|---|---|---|---|---|---|---|
| Initial Bayliss amplitude | 0.01 | 0.30 | 0.56 | 0.76 | 0.86 | 0.89 | 0.82 | 0.68 | 0.64 | 0.89 |
| | −0.01 | −0.30 | −0.56 | −0.76 | −0.86 | −0.89 | −0.82 | −0.68 | −0.64 | −0.89 |
| Fig.3(a) | | | | | | | | | | |
| Optimized amplitude | −0.01 | 0.30 | 0.56 | 0.76 | 0.86 | 0.89 | 0.82 | 0.68 | 0.64 | 0.89 |
| | −0.50 | −0.30 | −0.56 | −0.76 | −0.86 | −0.89 | −0.82 | −0.68 | −0.73 | −0.89 |
| Optimized phase (deg.) | 8.93 | 0.26 | 0.61 | 0.01 | 2.25 | 0.14 | −0.61 | 0.11 | −1.26 | −0.41 |
| | 0.04 | −89.11 | −0.26 | −0.83 | −0.30 | 0.04 | 0.13 | 0.42 | 0.09 | −0.90 |
| Fig.3(b) | | | | | | | | | | |
| Optimized amplitude | −0.01 | 0.30 | 0.56 | 0.76 | 0.86 | 0.89 | 0.82 | 0.68 | 0.64 | 0.89 |
| | −0.50 | −0.30 | −0.56 | −0.76 | −0.89 | −0.82 | −0.82 | −0.68 | −0.73 | −0.89 |
| Optimized phase (deg.) | 0.11 | 0.18 | 111.83 | 87.29 | 0.01 | 0.01 | 0.17 | 0.04 | 0.07 | −11.41 |
| | −37.24 | 0.01 | −0.04 | −0.23 | −0.02 | 0.02 | 0.02 | −0.10 | −0.06 | 93.62 |

As shown in Fig. 3(b), a side-lobe difference of $SD_d = 3.5$ dB is imposed. The final results show a side-lobe difference (SD) of 3.54 dB. On the other hand, the side-lobe level is raised slightly than the case without this constraint, as in the optimized pattern 4 in Table II). In practice, imposing the side-lobe level difference between the left and the right hand sides may not be necessary.

Next, consider a uniformly spaced linear array, consisted of 40 elements ($L_x = 20\lambda$ and $N_x = 20$). The amplitude distribution of a Bayliss array with $N_b = 10$ is used as the initial condition to optimize the difference field pattern. The parameters used in this simulation are also listed in Table I, except $N = 80$. Fig. 4 and Table II show the simulation results. Asymmetrical difference patterns with different PD's can be generated. The side-lobe difference is difficult to achieve, as in the previous case. In both cases, the side-lobe level away from the main beam is raised as a consequence of achieving a lower maximum side-lobe level.

Table III lists the amplitude and phase of excitations to achieve the optimized field pattern, as shown in Figs. 3(a) and (b). It is observed that the amplitudes are slightly different from the initial amplitudes of the Bayliss array. Also notice that the phase varies more wildly from element to element as $PD_d$ is increased.

Table IV lists the success rate (SR), the best fitness, the average fitness (avg. fitness) and the average iterations (avg. FI) of the PSO, MPSO, GA and MGA, respectively, all with 10 trials. The best fitness using the MPSO is not always the best among these four algorithms and it takes more fitness iterations. However, the success rate and the average fitness using the MPSO are better than those of the other algorithms. It seems difficult for the GA and the MGA to fully satisfy the constraints, expressed by the fitness function, to achieve the desired asymmetric difference pattern when the constraint $PD_d$ is increased. With a larger $PD_d$, the PSO algorithm renders a lower success rate and poorer average fitness than the MPSO.

TABLE IV
COMPARISON OF PSO, MPSO, GA, AND MGA USING PARAMETERS IN Table II

Optimized pattern 1

| algorithm | SR | best fitness (dB) | avg. fitness (dB) | avg. FI |
|---|---|---|---|---|
| PSO | 10/10 | −19.82 | −19.35 | **75,772** |
| MPSO | 10/10 | **−20.00** | **−19.65** | 118,915 |
| GA | 10/10 | −16.90 | −16.32 | 75,980 |
| MGA | 10/10 | −17.56 | −16.77 | 157,150 |

Optimized pattern 2

| algorithm | SR | best fitness (dB) | avg. fitness (dB) | avg. FI |
|---|---|---|---|---|
| PSO | 10/10 | −16.10 | −14.05 | **88,976** |
| MPSO | 10/10 | **−16.25** | **−15.04** | 110,898 |
| GA | 0/10 | none | none | none |
| MGA | 2/10 | −13.63 | −13.25 | 126,750 |

Optimized pattern 4

| algorithm | SR | best fitness (dB) | avg. fitness (dB) | avg. FI |
|---|---|---|---|---|
| PSO | 7/10 | **−9.49** | −6.86 | **64,309** |
| MPSO | **10/10** | −9.42 | **−8.16** | 92,060 |
| GA | 0/10 | none | none | none |
| MGA | 0/10 | none | none | none |

### B. Uniformly Excited Array as Initial Condition

Consider a uniformly spaced linear array, consisted of 20 elements ($L_x = 10\lambda$ and $N_x = 10$). The initial amplitudes of these elements

TABLE V
COMPARISON OF RESULTS IN Fig. 5

$N_x = 10$

| Source | $PD_d$ (dB) | $SA_d$ (deg.) | PD (dB) | SA (deg.) | BW (deg.) | SLL (dB) | SD (dB) |
|---|---|---|---|---|---|---|---|
| Initial uniformly excited pattern | none | none | 0.00 | 8.20 | 22.00 | −10.27 | 0.00 |
| Optimized pattern 1 | 0.00 | 8.00 | 0.00 | 8.00 | 19.50 | −19.56 | 0.00 |
| Optimized pattern 2 (Fig.5 (a)) | 1.00 | 8.00 | 1.00 | 8.00 | 19.00 | −15.53 | 0.01 |
| Optimized pattern 3 | 2.00 | 8.00 | 2.00 | 8.00 | 19.30 | −12.78 | 0.28 |
| Optimized pattern 4 | 4.00 | 8.00 | 4.00 | 8.00 | 19.50 | −8.86 | 0.05 |
| Optimized pattern 5 (Fig.5 (b)) | 4.00 | 8.00 | 4.00 | 8.00 | 18.60 | −8.45 | 3.51 |

TABLE VI
AMPLITUDES AND PHASES OF EXCITATION TO GENERATE THE FIELD PATTERN IN Fig. 5(a) and (b)

| | | | | | | | | | | |
|---|---|---|---|---|---|---|---|---|---|---|
| Initial uniformly excited amplitude | 1.00 | 1.00 | 1.00 | 1.00 | 1.00 | 1.00 | 1.00 | 1.00 | 1.00 | 1.00 |
| | −1.00 | −1.00 | −1.00 | −1.00 | −1.00 | −1.00 | −1.00 | −1.00 | −1.00 | −1.00 |
| | | | | | Fig. 5(a) | | | | | |
| Optimized amplitude | 1 | 0.68 | 1.00 | 1.00 | 1.00 | 1.50 | 1.00 | 0.99 | 1.00 | 0.74 |
| | −0.01 | −0.13 | −1.00 | −1.06 | −1.01 | −0.99 | −0.99 | −1.07 | −0.99 | −1.00 |
| Optimized phase (deg.) | −1.04 | 0.02 | 0.10 | −0.13 | 0.06 | −0.04 | 0.05 | −0.06 | −0.66 | −0.16 |
| | 0.00 | −0.12 | −63.76 | −0.12 | −0.03 | 0.24 | −0.06 | −3.25 | 2.41 | 0.31 |
| | | | | | Fig. 5(b) | | | | | |
| Optimized amplitude | 0.99 | 0.99 | 0.99 | 0.08 | 1.00 | 1.00 | 1.00 | 0.99 | 1.00 | 0.99 |
| | −1.40 | −0.99 | −1.00 | −0.98 | −0.99 | −0.51 | −0.95 | −0.99 | −1.02 | −1.00 |
| Optimized phase (deg.) | 0.16 | 1.31 | 83.13 | −0.27 | −0.03 | −0.05 | 0.34 | 0.14 | 0.01 | −0.36 |
| | −80.92 | −0.69 | 2.25 | −2.34 | 15.62 | −0.96 | 0.01 | −2.50 | −0.02 | 81.13 |

TABLE VII
COMPARISON OF PSO, MPSO, GA AND MGA USING PARAMETERS IN Table V

Optimized pattern 1

| algorithm | SR | best fitness (dB) | avg. fitness (dB) | avg. FI |
|---|---|---|---|---|
| PSO | 10/10 | −19.44 | −16.63 | **96,215** |
| MPSO | 10/10 | **−19.56** | **−17.65** | 159,420 |
| GA | 0/10 | none | none | none |
| MGA | 0/10 | none | none | none |

Optimized pattern 2

| algorithm | SR | best fitness (dB) | avg. fitness (dB) | avg. FI |
|---|---|---|---|---|
| PSO | 10/10 | −14.28 | −12.63 | **113,770** |
| MPSO | 10/10 | **−15.53** | **−13.32** | 165,738 |
| GA | 0/10 | none | none | none |
| MGA | 0/10 | none | none | none |

Optimized pattern 4

| algorithm | SR | best fitness (dB) | avg. fitness (dB) | avg. FI |
|---|---|---|---|---|
| PSO | 5/10 | −8.01 | −5.92 | **84,999** |
| MPSO | **6/10** | **−8.86** | **−7.91** | 147,310 |
| GA | 0/10 | none | none | none |
| MGA | 0/10 | none | none | none |

are the same; the initial phases of the right 10 elements are 0, while those of the left 10 elements are 180°.

The same optimization algorithms are applied. The simulation results are shown in Fig. 5 and summarized in Table V. Table VI lists the amplitude and phase of the excitations to generate the optimized field patterns, as shown in Figs. 5(a) and (b). Table VII lists the success rate, the best fitness, the average fitness and the average fitness iterations of the PSO, MPSO, GA and MGA algorithms, respectively, all with 10 trials. The MPSO performs well with the uniformly excited linear array as the initial condition, in terms of the success rate, the best fitness, and the average fitness.

By comparing Tables IV and VII, it appears that using the Bayliss array as the initial condition renders a better difference pattern and better optimization indices, especially the success rate and the average fitness.

## V. CONCLUSION

A memetic particle swarm optimization (MPSO) algorithm is applied to optimize the amplitudes and phases of a uniformly spaced linear array, to generate an asymmetrical difference pattern. The difference patterns have been simulated for linear arrays with 20 and 40 elements, respectively, with constraint on the peak difference. The side-lobe level can be suppressed while maintaining the desired squint angle and the side-lobe difference. The MPSO renders better performance than the PSO, the genetic algorithm (GA) and the memetic GA (MGA), in success rate and average fitness, due to its hybrid mechanisms of global search and local search. The initial condition of amplitudes derived from a continuous Bayliss array proves to accelerate the convergence and further improve the optimization results.

## REFERENCES

[1] B. Edde, *Radar: Principles, Technology, Applications*. Englewood Cliffs, NJ, USA: Prentice-Hall, 1993, pp. 49–50.

[2] M. Satyanarayana and G. S. N. Raju, "Generation of asymmetrical difference patterns from array antennas," *Int. J. Electron. Telecommun.*, vol. 57, no. 2, pp. 185–190, Jul. 2011.

[3] S. Caorsi, A. Massa, M. Pastorino, and A. Randazzo, "Optimization of the difference patterns for monopulse antennas by a hybrid real/integer-coded differential evolution method," *IEEE Trans. Antennas Propag.*, vol. 53, no. 1, pp. 372–376, Jan. 2005.

[4] L. Manica, P. Rocca, A. Martini, and A. Massa, "An innovative approach based on a tree-searching algorithm for the optimal matching of independently optimum sum and difference excitations," *IEEE Trans. Antennas Propag.*, vol. 56, no. 7, pp. 58–66, Jan. 2008.

[5] P. Rocca, L. Manica, and A. Massa, "An improved excitation matching method based on an ant colony optimization for suboptimal-free clustering in sum-difference compromise synthesis," *IEEE Trans. Antennas Propag.*, vol. 57, no. 8, pp. 2297–2306, Aug. 2009.

[6] P. Rocca, G. Oliveri, and A. Massa, "Differential evolution as applied to electromagnetics," *IEEE Antennas Propag. Mag.*, vol. 53, no. 1, pp. 38–49, Feb. 2011.

[7] J. Robinson and Y. Rahmat-Samii, "Particle swarm optimization in electromagnetics," *IEEE Trans. Antennas Propag.*, vol. 52, no. 2, pp. 397–407, Feb. 2004.

[8] R. L. Haupt, "Thinned arrays using genetic algorithms," *IEEE Trans. Antennas Propag.*, vol. 42, no. 1, pp. 993–999, Jul. 1994.
[9] V. Murino, A. Trucco, and C. S. Regazzoni, "Synthesis of unequally spaced arrays by simulated annealing," *IEEE Trans. Signal Process.*, vol. 44, no. 1, pp. 119–123, Jan. 1996.
[10] D. G. Kurup, M. Himdi, and A. Rydberg, "Synthesis of uniform amplitude unequally spaced antenna arrays using the differential evolution algorithm," *IEEE Trans. Antennas Propag.*, vol. 51, no. 9, pp. 2210–2217, Sep. 2003.
[11] M. M. Khodier and C. G. Christodoulou, "Linear array geometry synthesis with minimum sidelobe level and null control using particle swarm optimization," *IEEE Trans. Antennas Propag.*, vol. 53, no. 8, pp. 2674–2679, Aug. 2005.
[12] O. Quevedo-Teruel and E. Rajo-Iglesias, "Ant colony optimization in thinned array synthesis with minimum sidelobe level," *IEEE Antennas Wireless Propag. Lett.*, vol. 5, pp. 349–352, 2006.
[13] G. Oliveri and A. Massa, "GA-enhanced ADS-based approach for array thinning," *IET Microwave Antennas Propag.*, vol. 5, pp. 305–315, Feb. 2011.
[14] G. Oliveri, F. Caramanica, and A. Massa, "Hybrid ADS-based techniques for radio astronomy array design," *IEEE Trans. Antennas Propag.*, vol. 59, no. 6, pp. 1817–1827, Jun. 2011.
[15] P. Moscato, On Evolution, Search, Optimization, Genetic Algorithms and Martial Arts: Toward Memetic Algorithms CalTech, Pasadena, CA, Rep. 826, 1989, Caltech Concurrent Computation Program.
[16] S. Caorsi, A. Massa, M. Pastorino, M. Raffetto, and A. Randazzo, "Detection of buried inhomogeneous elliptic cylinders by a memetic algorithm," *IEEE Trans. Antennas Propag.*, vol. 51, no. 10, pp. 2878–2884, Oct. 2003.
[17] Y. Petalas, K. Parsopoulos, and M. Vrahatis, "Memetic particle swarm optimization," *Ann. Oper. Res.*, vol. 156, pp. 99–127, 2007.
[18] T. A. Milligan*, Modern Antenna Design*, 2nd ed. New York, NY, USA: Wiley-Interscience, 2005, pp. 158–164.
[19] R. J. Mailloux*, Phased Array Antenna Handbook*, 2nd ed. Norwood, MA, USA: Artech House, 2005, pp. 132–133.
[20] Y. T. Lo and S. W. Lee*, Antenna Handbook*. New York, NY, USA: Van Nostrand Reinhold, 1988, pp. 13–29.
[21] A. Hoorfar, "Evolutionary programming in electromagnetic optimization: A review," *IEEE Trans. Antennas Propag.*, vol. 55, no. 3, pp. 523–537, Mar. 2007.
[22] S. Xu and Y. Rahmat-Samii, "Boundary conditions in particle swarm optimization revisited," *IEEE Trans. Antennas Propag.*, vol. 52, no. 3, pp. 760–765, Mar. 2007.

# Electronically Reconfigurable Liquid Crystal Based Mm-Wave Polarization Converter

E. Doumanis, G. Goussetis, R. Dickie, R. Cahill, P. Baine, M. Bain, V. Fusco, J. A. Encinar, and G. Toso

***Abstract*—An electronically tunable reflection polarizer which exploits the dielectric anisotropy of nematic liquid crystals (LC) has been designed, fabricated and measured in a frequency band centered at 130 GHz. The phase agile polarizing mirror converts an incident slant 45° signal upon reflection to right hand circular (RHCP), orthogonal linear ($-45°$) or left hand circular (LHCP) polarization depending on the value of the voltage biasing the LC mixture. In the experimental set-up this is achieved by applying a low frequency bias voltage of 0 V, 40 V and 89 V respectively, across the cavity containing the LC material.**

***Index Terms*—Earth observation, imaging, interferometry, liquid crystals, mm-wave, polarimetric systems, polarizer, remote sensing, space communications, submm-wave, tunable.**

## I. Introduction

Satellite polarimetric imaging systems, such as those used for passive and active Earth observation to measure the surface wind vector from space [1], [2] and vegetation properties [3], commonly involve dedicated receive and transmit chains for each polarization state. Tunable polarizers can reduce redundancy, volume/mass budget and cost. Dynamic polarization agility is also desirable in radar applications for defense and remote sensing to enhance detection and measurement of a feature in a radar scene [4] as well as wireless and satellite telecommunications to minimize feed losses and polarization purity impairments. Polarization agility in quasi-optical mm-wave systems can also be used to create tunable isolators (switches) [5] as well as frequency tunable interferometers for filtering and diplexing [6].

Traditional tunable polarizer technology relies on mechanical motors or rotors [4] leading to increased energy consumption and mass as well as compromised reliability. In order to address such limitations, integrated solutions based on, e.g., MEMS [7] and piezoelectric ultrasonic motors [8] have been proposed. Despite their compact physical dimensions, these technologies are suitable for switched-based architectures offering discrete polarization states. Moreover, such technologies are mostly relevant to waveguide-based polarizers which are difficult to scale to (sub)mm-wave frequencies; free-space polarizers would

Manuscript received August 29, 2013; revised November 22, 2013; accepted December 30, 2013. Date of publication January 27, 2014; date of current version April 03, 2014. This work was supported by the European Space Agency under project 4000103061. The work of G. Goussetis was supported by FP7 project DORADA (IAPP-2013-610691) and the European Space Agency (grant A0/1-6169/09/NL/JD).

E. Doumanis is with Bell-Labs Alcatel-Lucent, Blunchardstown Industrial Park, Dublin 15, Ireland (e-mail: efstratios.doumanis@alcatel-lucent.com)

G. Goussetis is with the School of Engineering and Physical Sciences, Heriot-Watt University, Edinburgh EH14 4AS, U.K. (e-mail: g.goussetis@ieee.org)

R. Dickie, R. Cahill, P. Baine, M. Bain, and V. Fusco are with the Institute of Electronics, Communications and Information Technology, Queen's University Belfast, Belfast BT3 9DT, Northern Ireland, U.K. (e-mail: r.cahill@qub.ac.uk)

J. A. Encinar is with the Department of Electromagnetism and Circuit Theory, Universidad Politécnica de Madrid, E-28040, Madrid, Spain (e-mail: jose.encinar@upm.es).

G. Toso is with the European Space Agency ESA–ESTEC, 2200 AG Noordwijk, The Netherlands (e–mail: giovanni.toso@esa.int).

Color versions of one or more of the figures in this communication are available online at http://ieeexplore.ieee.org.

Digital Object Identifier 10.1109/TAP.2014.2302844